JCTC Journal of Chemical Theory and Computation
Letter
pubs.acs.org/JCTC

Rapid Conformational Fluctuations of Disordered HIV-1 Fusion Peptide in Solution

Tom Venken,[†] Arnout Voet,[†] Marc De Maeyer,[†] Gianni De Fabritiis,*[,‡] and S. Kashif Sadiq*[,‡]

[†]Laboratory for Biomolecular Modelling and BioMacS, Department of Chemistry, Division of Biochemistry, Molecular and Structural Biology, KU Leuven, Celestijnenlaan 200G box 2403, 3001 Heverlee, Belgium

[‡]Computational Biophysics Laboratory (GRIB-IMIM), Universitat Pompeu Fabra, Barcelona Biomedical Research Park (PRBB), C/Doctor Aiguader 88, 08003 Barcelona, Spain

Supporting Information

ABSTRACT: The conformationally flexible fusion peptide (FP) of HIV-1 is indispensible for viral infection of host cells, due to its ability to insert into and tightly couple with phospholipid membranes. There are conflicting reports on the membrane-associated structure of FP, and solution structure information is limited, yet such a structure is the target for a novel class of antiretroviral inhibitors. An ensemble of explicit solvent molecular dynamics simulations, initiated from a disordered HIV-1 FP (aggregate time of ∼30 μs), revealed that while the vast majority of conformations predominantly lack secondary structure, both spontaneous formation and rapid interconversion of local secondary structure elements occur, highlighting the structural plasticity of the peptide. Therefore, even at this rapid time scale, FP constitutes a diverse and flexible conformational ensemble in solution. Secondary structure clustering reveals that the most prominent ordered elements are α- and 3−10-helical subsets of membrane-bound conformations, while trace populations within 2 Å RMSD of all complete membrane-bound conformations are found to pre-exist in the solution ensemble. Since inhibitor bound conformations of FP are only rarely found, FP inhibitors could function by modulating the conformational ensemble and binding to nonfusogenic FP structures. A thermodynamic characterization of the most prominent ordered nonfusogenic structures could facilitate the future design of improved FP inhibitors.

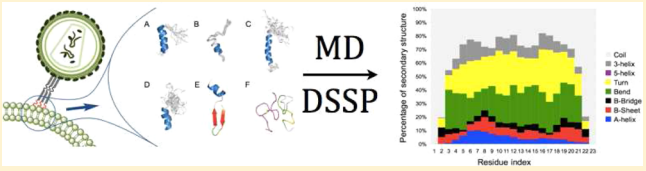

Fusion of viral and host cell membranes is an essential *modus operandi* to achieve infection for many enveloped viruses, including HIV and influenza.[7,8] In HIV, recognition of viral envelope protein gp120 by host-cell receptors triggers multiple conformational changes in the neighboring viral protein, gp41, leading to a coiled trimer of α-helices and the exposure of a highly conserved trimeric 23 amino acid gp41 N-terminal fusion peptide (FP), which is inserted into the host membrane via a harpoon mechanism that initiates membrane fusion (Figure 1).

Structural characterization of FP has been attempted with several experimental techniques.[1−4,9−13] Nevertheless, contradictory results have been found regarding the secondary structure of the peptide in its membrane-associated form, ranging from either α-helical,[3] β-sheet,[10] or irregular unstructured conformations[9] or a combination of these.[1,2,4,11,12]

It has been suggested that the fusogenic form is a transient flexible structure, not a stable α-helical or β-sheet conformation.[9] Another possibility is that both α-helical and β-sheet structures are fusogenic,[13] or that an α-helical structure predominates in solution, which transitions into mainly β-sheets in the membrane after insertion.[12] Recently, EPR experiments suggested the transition of the inserted FP from a β-sheet in lipid raft regions to an α-helix conformation in the course of membrane fusion.[13] This indicates that the FP may be an intrinsically disordered peptide representing a high structural plasticity, which can adopt multiple conformations depending on its vicinal environment.[8]

Most attempts to characterize the FP have been in membrane-bound form (Figure 1A−E),[1−5] of which several have been shown to be stable in membrane simulations.[5,11,14−16] Despite this, characterization of HIV-1 FP in solution may be of crucial importance in understanding the fusogenic process. Furthermore, the recently discovered VIRus INhibitory Peptide (VIRIP) and its optimized derivatives (e.g., VIR-165 and VIR-576) block viral entry by binding to a disordered conformation of FP (Figure 1F).[6,17] Thus, structural characterization of the conformational ensemble of FP in solution is of great pharmacological importance if *a priori* predictions of solution structure can be made. We find that none of the membrane bound structures is stable in solution and that FP undertakes rapid fluctuations including α-helix and β-sheet secondary structure elements, dynamics which are compatible with a disordered protein.

Our aim was to gain insight into the propensity to form secondary structure elements as well as to qualitatively establish whether any significant structural plasticity of HIV-1 FP is exhibited in solution; thus we used a classical molecular simulation methodology.

Received: October 3, 2012
Published: May 20, 2013

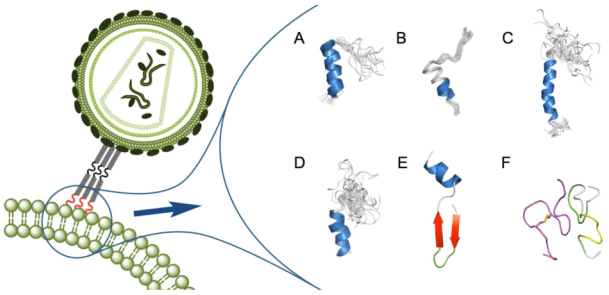

Figure 1. Schematic representation of HIV-1 fusion and overview of the experimentally determined structures of gp41 FP in membrane-like environments or solution. After recognition of the host cell-membrane CD4 receptor and coreceptors by the gp120 protein (hidden for clarity), the trimeric gp41 protein (gray) undergoes a conformational rearrangement, thereby exposing and inserting the gp41 FP (red) in the host cell membrane. The inlet on the right displays some of the proposed structures of gp41 FP (A–F). (A) α-helical FP23 with FTIR restraints in hexafluoroisopropanol (PDB-code: 1ERF).[1] (B) α-helical FP23 with FTIR restraints in SDS micelles (PDB-code: 1P5A).[2] (C) Solution NMR α-helical FP30 (PDB-code: 2ARI).[3] (D) Solution NMR α-helical FP23 (PDB-code: 2PJV).[4] (E) β-sheet model FP23 (model based on PDB-code: 3D58).[5] (F) Solution NMR unstructured FP23 in complex with VIR-165 (pink), a disulfide stabilized derivative of the fusion peptide inhibitor VIRIP (PDB-code: 2JNR).[6] FP secondary structures are colored according to the DSSP convention with blue, α-helix; red, β-sheet; white, coil; black, β-bridge; green, bend; yellow, turn; purple, π-helix; and gray, 3–10-helix.

All-atom explicit solvent molecular dynamics simulations using ACEMD[18] on local computer resources were performed starting from each of the conformations A–F shown in Figure 1 up to a production time of 300 ns. Furthermore, a larger ensemble of simulations (94 × 300 ns) was performed on the GPUGRID infrastructure,[19] starting from a completely unstructured peptide chain, with the highest prevalence HIV-1 FP sequence, AVGIGALFLGFLGAAGSTMGARS, denoted FP23. The recently improved AMBER force-field, ff99SBildn, was used to describe all parameters.[20] The TIP3P water model was used for solvation, and the systems were electrically neutralized at an ionic concentration of 150 mM NaCl. See the Supporting Information (SI) for simulation details.

Peptide structure was characterized with the Define Secondary Structure of Proteins (DSSP) method.[21] The following secondary structure elements are defined: α-helix, β-sheet, coil, β-bridge, bend, turn, π-helix, and 3–10-helix for each amino acid. Root mean squared deviations (RMSDs) of corresponding subsets of C_α atoms were also calculated with respect to the conformations A–F with prior fitting to corresponding secondary structural features (SI).

All simulations of FP in solvent from each of the conformations A–F show rapid decay of their respective secondary structure features into unstructured conformations within the 20 ns period of equilibration and specifically as soon as constraints are removed (SI: Figure S1). Furthermore, a lack of ordered features persists for most systems across 300 ns of simulation. RMSD calculations with respect to the initial secondary structural features of each structure are consistent with the DSSP calculations.

We investigated whether any of the structural features found in structures A–F can pre-exist in solution, by performing simulations (94 × 300 ns) from multiple initial unstructured conformations of FP23. We determined the RMSD distribution of the entire ensemble with respect to each of the specific secondary structural features corresponding to the experimental conformations (Figure 2). Most conformations in our solution

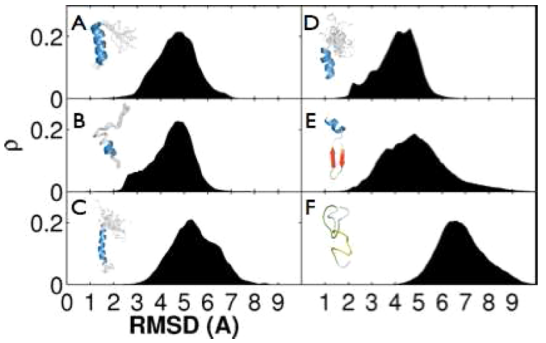

Figure 2. RMSD distribution of the conformational ensemble of FP with respect to corresponding experimental/model FP structures (A–F), respectively.

ensemble deviate strongly from the FP23 structures found in membrane-like environments (Figure 2A–E) with peak RMSDs between 5 and 6 Å compared to secondary structural features. Nevertheless, a small percentage of structures within the ensemble were found within 2 Å RMSD of conformations A–D (A, 0.21%; B, 0.05%; C, 0.01%; D, 0.49%), while conformation E was not present. Interestingly, when comparing RMSD relative to either the α (residues 15–22) or β (residues 2–5 and 9–12) components of structure E separately, 0.21% and 6.38% of conformations were within this RMSD threshold, respectively (RMSD distribution for E shown in Figure 2 corresponds to a comparison with the β-sheet only). The mean deviation from structure F (VIR-165 bound apo-form of FP) was ~7 Å, and no conformations were present below a 2 Å RMSD threshold, the minimum being at 3 Å. Only 0.01% were within 3.5 Å RMSD. This is not surprising as conformation F has no significant secondary structural features (only bends and turns), so RMSD was calculated with respect to all C_α atoms within the chain.

Calculating the proximity distribution in DSSP state space resulted in a similar trend, displaying the rare occurrence of structures matching the experimental structures (SI: Figures S2 and S3). Thus, although the majority of solution conformations vastly differs from the membrane conformations, some membrane-like structures infrequently seem to pre-exist in solution. In addition, a small number of coiled structures similar to the VIR-165-bound conformation were found (SI: Figure S3).

We attempted to distinguish the different conformations found within the ensemble. Singular metrics such as RMSD with respect to key structures and the radius of gyration provide insufficient discrimination between the multitude of secondary structural features that can arise and provide only global properties of structural characterization (SI: Figure S4). Therefore, DSSP was used to analyze secondary structure variance within the ensemble.

The overall propensity to form any given secondary structure element was calculated both as an average across the entire peptide (termed global DSSP propensity) and on a per residue basis. Block-averaging across all trajectories showed an equilibration of the global DSSP propensity at 150 ns (SI: Figure S5). The latter 94 × 150 ns was therefore used for reporting global and per residue structural propensities.

dx.doi.org/10.1021/ct300856r | J. Chem. Theory Comput. 2013, 9, 2870–2874

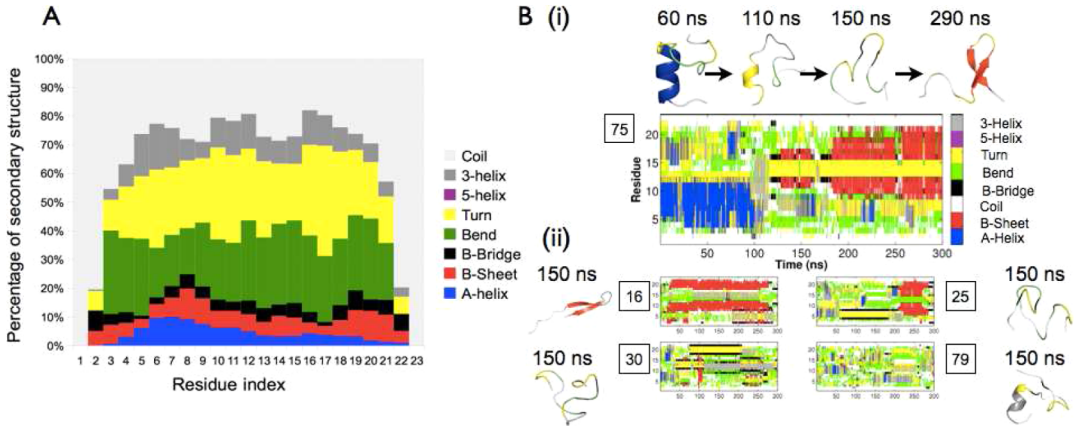

Figure 3. (A) Percentage of secondary structure averaged over all trajectories and calculated per residue. Structural color scheme is blue, α-helix; red, β-sheet; white, coil; black, β-bridge; green, bend; yellow, turn; purple, π-helix; and gray, 3−10-helix. (B) Selected examples of trajectories with different secondary structure elements in DSSP representation. Simulation 75: conversion of α-helical to β-sheet conformation. Simulation 16: trajectory with a high β-sheet content. Simulation 25: trajectory with a combination of β-bridges and β-sheets. Simulation 30: trajectory with a combination of multiple β-bridges and 3-helices. Simulation 79: trajectory with a high amount of coiled conformations and only a limited amount of secondary structure. Representative structures during the trajectories are shown beside the DSSP graphs, with the secondary structure of the FP in DSSP colors.

DSSP analysis shows that FP23 is predominantly unstructured or exhibits locally stabilized structures such as bends and turns in the solution ensemble (Figure 3A). Coiled conformations have a high frequency (average of 38.1%) which is mainly manifested in the terminal residues. Moreover, a high concentration of bends (average of 19.7%) and turns (average of 20.6%) is present in the entire structure. Extended secondary structure elements are found as well, though at lower percentages. A modest amount of 3−10-helices (average of 7.9%) was found in the FP23 structure, while the propensity of the π-helix is insignificant (average of 0.1%).

In contrast, a small degree of α-helix formation (average of 4.0%) was detected, mostly between residues Gly5 and Leu12. Interestingly, the higher α-helical content between residues Gly5 and Leu12 as compared to the other residues has been suggested previously using a secondary structure prediction program[22] and is consistent with the results of an α-helical prediction algorithm[23] (SI: Figure S6). There is also a moderate propensity of β-sheet conformations (average of 5.7%) or isolated β-bridges (average of 3.9%) in the solvent as well. Combining all helical (α-helix, 3−10-helix, and π-helix) and β-sheet conformations (β-sheet and β-bridge) results in a slightly larger tendency to form helices (average of 11.9%) than β-sheet like structures (average of 9.6%). Nevertheless, these fractions are much lower than the unstructured conformations coil, bend, and turn taken together (average of 78.4%).

We next compared the secondary structure predictions with previous experiments. Transmission FTIR measurements of FP23 in deuterated buffer solution indicated a mixture of molecular aggregates of intermolecular β-sheet structures and unordered + helical conformations.[12] FTIR measurements of FP23 in phosphate buffer showed α-helix, β-sheet, β-bridge, and coil estimations of respectively 20.1%, 40.4%, 19.5%, and 20%.[24] EPR spectra of nitroxide spin labels attached to N-terminal and C-terminal residues showed a high rotation rate, underlining the flexibility of the coiled conformations of FP in solution.[13] These reduced significantly when probing lipid environments. Coiled conformations in aqueous solvent have been found for other fusion peptides as well, such as the influenza FP.[25] In addition, a secondary structure prediction study performed before[22] showed α-helix, β-sheet, and coil probabilities of respectively 40%, 7%, and 53%. Furthermore, several protein disorder prediction methods indicate that the peptide could be disordered (SI: Figure S7).

The quantitative deviation with our calculations may be for a number of reasons. First, single FP molecules were simulated here while interactions between multiple FP molecules occur in experiments. For example, interstrand β-sheets and other interresidual stabilizations are absent in our simulations, which could explain the higher β-sheet content in the FTIR experiments. We hypothesize that conformational experiments on single FPs would result in lower β-sheet content and partially explain the role of FP multimerization. Second, simulations may be sensitive to the cutoff used to describe various intramolecular interactions.[26] Furthermore, the Amber force-field, ff99SBildn, is known to slightly underestimate the α-helical content in MD simulations.[27] Use of a more accurate force-field may thus reduce the observed discrepancy. Finally, while the secondary structure prediction shows a majority of coil probabilities (53%), a large amount of α-helix was predicted as well (40%), which is much higher than in our MD simulations and in the FTIR experiments. Secondary structure prediction algorithms are usually optimized for larger proteins which also contain tertiary structures. In contrast, the FP with only 23 amino acids is too small to contain a tertiary fold, which could influence the reliability of the secondary structure prediction.

On the other hand, we note that the amount of α-helix measured in experiments may be exaggerated because these involve ensemble measurements averaged in time. Sometimes helical structures can be detected in experiments, though these structures actually could be highly averaged random-flight chains, containing mostly bends, turns, and coils instead.[28] Previous studies on the alanine-based XAO peptide, a model for the unfolded state of proteins,[29] show it to display a very flexible, fluctuating structure that only seldom adopts a helical conformation, quite similar to the behavior of FP23.

Analysis of the time evolution of secondary structural features across all trajectories reveals a detailed account of the specific conformational ensemble and structural inter-

conversions (SI: Figure S8). Strong variations exist between different simulations but also within a single trajectory, clearly demonstrating the inherent structural plasticity of FP23.

Most simulations reveal a high quantity of unstructured conformations. This notion is demonstrated by simulation 79 (Figure 3B), for example, where mostly coil, bend, and turn are exhibited. The secondary structures also display a persistence time of only a few nanoseconds. In contrast, simulation 16 clearly illustrates the formation of a stable C-terminal β-sheet structure, which persists for around 250 ns, though it unfolds again at the end of the simulation.

The formation of stable β-sheets is not restricted to these specific residues as shorter β-sheets have also been observed, for example, in simulation 75. Isolated β-bridges were found regularly as well, like in simulation 25. This local structure lasts for more than 100 ns until it unfolds and then forms a transient β-sheet. β-bridges can be found in almost all residues except for termini. Simulation 30 for example contains multiple temporary β-bridges at different time points.

In simulation 75, an α-helix with a persistence time of ∼100 ns converts into a β-sheet structure that lasts to the end of the simulation via transitional 3−10 helix and β-bridge conformations (Figure 3B and SI Movie M1). This example clearly demonstrates the high secondary structure plasticity of FP23 in solution, as stable α-helix, β-sheet, and coiled unfolded structures can occur in just a few hundred nanoseconds.

The ensemble was clustered in DSSP space (SI: Figures S9) using a k-means clustering algorithm. Filtering of the most frequent secondary structure elements in each cluster (frequency >0.8) and then highlighting those clusters which had low mean RMSDs (<0.75 Å) relative to the average filtered secondary structure element revealed that the most prevalent and stable conformations in the ensemble are first N- and then C-terminal α-helices or closely related 3−10-helices. N- and C-terminal β-sheets also exist in conformations but not to the same degree of prevalence or stability (SI: Figures S10). The most relevant stable elements thus are subsets of the α-helical forms of membrane-bound fusion peptide. These structures are provided in the SI.

The conventional paradigm of structure-based function in proteins has been challenged in recent years by the realization that many proteins exist in a disordered yet functional state.[30,31] These intrinsically disordered proteins (IDPs) exist in a conformational equilibrium of states with low interconversion energy barriers,[32] others become spontaneously ordered in response to triggered binding events.[33] In addition, the entire protein can be disordered, or only selected regions can adopt a disordered conformation.

Our results suggest that, on this time scale, HIV-1 FP is mainly disordered and constitutes a diverse, flexible, and rapidly interconverting conformational ensemble in solution. However, it remains unclear whether FP23 displays a similar flexibility when attached to the much larger gp41 protein or in its oligomerized state. Crystal structures of gp41 either exclude FP due to its hydrophobicity decreasing solubility and/or because of its flexibility. Nonetheless, we postulate that FP23 as part of a much larger gp41 protein *in vivo* is likely to be disordered based on (a) the disorder exhibited in free FP23 in our study, (b) the fact that several crystal structures of gp41 are not resolved even upon inclusion of the first 23 N-terminal residues (for example PDB-codes 2X7R and 3P30), (c) the fact that, to our knowlegde, in the only crystal structure where a fusion peptide has been resolved, that of influenza haemagglutinin in complex with an inhibitor (PDB-code: 3EYJ, chain B), the FP is indeed disordered, and (d) several protein disorder prediction methods indicate that the peptide could be disordered (SI: Figure S10). In fact, it has been suggested previously that viral fusion peptides may form autonomous folding units in the membrane.[25] We propose that future simulations of gp41 including fusion peptide will be able to test this hypothesis.

Intriguingly, most IDPs are characterized by a high concentration of polar amino acids, yet FP23 lacks these, except for Ser117, Thr118, and Arg122 in the C-terminus. Nevertheless, FP23 has a high fraction of Ala and Gly residues, which are known for disorder inducing tendencies.[34] The conformational ensemble will evidently be different upon oligomerization and upon attachment to the entire gp41 protein, which will influence long-range interactions. Nonetheless, the FP23 as such is inserted into the membrane in a monomeric form and is only oligomerized after conformational change of gp41 into a six-helix bundle,[7] warranting the analysis of FP23 in its monomeric form to understand membrane insertion.

Recently, an acid-denatured 80 amino acid ACPB protein which has a natural tertiary fold was found to maintain residual ordering and slow interconversions across a long time scale of 200 μs.[35] Our findings cannot rule out the possibility of stable solution structures with relaxation times >30 μs. Such structures would not conform to existing membrane-bound conformations, although they might be composed of a combination of the secondary structural elements identified in our study. However, FP23 is four times smaller than ACPB, lacks a tertiary fold, and even structured proteins of slightly larger size fold at significantly shorter time scales,[36] suggesting that a stable solution structure of FP23 at longer time scales is unlikely.

Our work opens up future studies that could elucidate the conformational modulation of FP (a) upon formation of a trimer, (b) in the transition from solvent to membrane environment, and (c) upon inhibitor binding. The transition from solvent to membrane-bound FP as well as formation of the FP trimer may be crucial in fully understanding the nature of fusogenicity. Importantly, our results show that the key secondary structural features of experimentally observed membrane bound structures are not substantially populated within the solution ensemble due to a large diversity of disordered states, although they partially overlap with the most prevalent of the small minority of ordered conformations. A full kinetic treatment of conformational change upon membrane association, analogous to kinetic studies of fast-folding proteins,[37,38] protein autocatalysis,[39] and enzyme inhibitor binding[40] would, in principle, determine the degree to which both conformational selection and induced fit account for FP membrane insertion and stabilization. Large-scale simulation of several FPs may determine whether FP readily oligomerizes in solution and whether specific conformations facilitate this process.

Our findings suggest that the FP inhibitor VIRIP, which binds a nonfusogenic structure, may function by modulating the conformational ensemble of FP. A comprehensive view of conformational modulation acknowledges the existence of a distribution of conformations even among the drug-bound states of a protein.[32,41,42] The VIRIP bound structure and those that are proximal to it also pre-exist within the solution ensemble, yet occur seldomly. Stabilization of these structures upon VIRIP binding may shift the conformational equilibrium

away from fusogenic structures that coexist in solution. This would partially explain the high dose requirements of VIRIP in experiments and clinical trials,[17] and future investigations may establish this shift quantitatively.

Finally, we suggest an improved strategy to guide the design of new inhibitors which focuses on extracting the minority of prevalent ordered elements in the ensemble as potential targets. However, as the most prevalent of these partially overlap with the membrane-bound N-terminal α-helical structures, inhibitors targeting such structures would primarily need to disrupt subsequent membrane insertion and/or FP multimerization. An alternative FP inhibitor design strategy may thus be to thermodynamically characterize the most prominent ordered nonfusogenic structures as targets for inhibition.

■ ASSOCIATED CONTENT

Supporting Information

Detailed methods; raw data of DSSP time evolution; analyses of decay of membrane-bound structure in solvent, conformational changes, average trend of secondary structure features, helical content, protein disorder prediction, and conformational clustering; available solution structures; and a movie of conformational plasticity. This material is available free of charge via the Internet at http://pubs.acs.org.

■ AUTHOR INFORMATION

Corresponding Author

*E-mail: syedkashifsadiq@gmail.com; gianni.defabritiis@upf.edu.

Notes

The authors declare no competing financial interest.

■ ACKNOWLEDGMENTS

The authors thank Prof. Dr. Jan Münch, Prof. Dr. Frank Kirchhoff, and Dr. Toni Giorgino for reading the manuscript and their useful suggestions. The authors are grateful to the volunteers of GPUGRID who donated GPU computing time to the project. The authors thank Prof. Dr. Robert C. Rizzo for sharing a gp41 protein model with the FP in antiparallel β-sheet conformation. T.V. acknowledges support from the Flemish Government through the concerted action scheme (GOA) and from the department of Chemistry, KU Leuven. G.D.F. acknowledges support from the Ramón y Cajal scheme, Acellera Ltd. and from the Spanish Ministry of Science and Innovation (ref. BIO2011-27450). S.K.S. acknowledges support from a European Commission FP7 Marie Curie Intra-European Fellowship.

■ REFERENCES

(1) Gordon, L. M.; Mobley, P. W.; Pilpa, R.; Sherman, M. A.; Waring, A. J. *Biochim. Biophys. Acta* **2002**, *1559*, 96−120.
(2) Gordon, L. M.; Mobley, P. W.; Lee, W.; Eskandari, S.; Kaznessis, Y. N.; Sherman, M. A.; Waring, A. J. *Protein Sci.* **2004**, *13*, 1012−1030.
(3) Jaroniec, C. P.; Kaufman, J. D.; Stahl, S. J.; Viard, M.; Blumenthal, R.; Wingfield, P. T.; Bax, A. *Biochemistry* **2005**, *44*, 16167−16180.
(4) Li, Y.; Tamm, L. K. *Biophys. J.* **2007**, *93*, 876−885.
(5) McGillick, B. E.; Balius, T. E.; Mukherjee, S.; Rizzo, R. C. *Biochemistry* **2010**, *49*, 3575−3592.
(6) Münch, J.; et al. *Cell* **2007**, *129*, 263−275.
(7) Doms, R. W.; Moore, J. P. *J. Cell Biol.* **2000**, *151*, F9−14.
(8) Epand, R. *Biochim. Biophys. Acta* **2003**, *1614*, 116−121.
(9) Grasnick, D.; Sternberg, U.; Strandberg, E.; Wadhwani, P.; Ulrich, A. S. *Eur. Biophys. J.* **2011**, *40*, 529−543.
(10) Qiang, W.; Sun, Y.; Weliky, D. P. *Proc. Natl. Acad. Sci. U. S. A.* **2009**, *106*, 15314−15319.
(11) Barz, B.; Wong, T.; Kosztin, I. *BBA* **2008**, *1778*, 945−953.
(12) Buzón, V.; Padrós, E.; Cladera, J. *Biochemistry* **2005**, *44*, 13354−13364.
(13) Lai, A. L.; Moorthy, A. E.; Li, Y.; Tamm, L. K. *J. Mol. Biol.* **2012**, *418*, 3−15.
(14) Kamath, S.; Wong, T. C. *Biophys. J.* **2002**, *83*, 135−143.
(15) Taylor, A.; Sansom, M. S. P. *Eur. Biophys. J.* **2010**, *39*, 1537−1545.
(16) Promsri, S.; Ullmann, G. M.; Hannongbua, S. *Biophys. Chem.* **2012**, *170*, 9−16.
(17) Forssmann, W. G.; et al. *Sci. Transl. Med.* **2010**, *2*, 63re3−63re3.
(18) Harvey, M. J.; Giupponi, G.; Fabritiis, G. D. *J. Chem. Theory Comput.* **2009**, *5*, 1632−1639.
(19) Buch, I.; Harvey, M. J.; Giorgino, T.; Anderson, D. P.; De Fabritiis, G. *J. Chem. Inf. Model.* **2010**, *50*, 397−403.
(20) Lindorff-Larsen, K.; Piana, S.; Palmo, K.; Maragakis, P.; Klepeis, J. L.; Dror, R. O.; Shaw, D. E. *Proteins* **2010**, *78*, 1950−8.
(21) Kabsch, W.; Sander, C. *Biopolymers* **1983**, *22*, 2577−2637.
(22) Venken, T.; Krnavek, D.; Münch, J.; Kirchhoff, F.; Henklein, P.; De Maeyer, M.; Voet, A. *Proteins* **2011**, *79*, 3221−3235.
(23) Lacroix, E.; Viguera, A.; Serrano, L. *J. Mol. Biol.* **1998**, *284*, 173−191.
(24) Gordon, L. M.; Nisthal, A.; Lee, A. B.; Eskandari, S.; Ruchala, P.; Jung, C.-L.; Waring, A. J.; Mobley, P. W. *Biochim. Biophys. Acta* **2008**, *1778*, 2127−2137.
(25) Han, X.; Bushweller, J. H.; Cafiso, D. S.; Tamm, L. K. *Nat. Struct. Biol.* **2001**, *8*, 715−720.
(26) Piana, S.; Lindorff-Larsen, K.; Dirks, R.; Salmon, J.; Dror, R.; Shaw, D. *PloS One* **2012**, *7*, e39918.
(27) Best, R. B.; Hummer, G. *J. Phys. Chem. B* **2009**, *113*, 9004−9015.
(28) Zagrovic, B.; Pande, V. S. *Nat. Struct. Biol.* **2003**, *10*, 955−961.
(29) Zagrovic, B.; Lipfert, J.; Sorin, E. J.; Millett, I. S.; van Gunsteren, W. F.; Doniach, S.; Pande, V. S. *Proc. Natl. Acad. Sci. U. S. A.* **2005**, *102*, 11698−11703.
(30) Dunker, A. K.; Silman, I.; Uversky, V. N.; Sussman, J. L. *Curr. Opin. Struct. Biol.* **2008**, *18*, 756−764.
(31) Mészáros, B.; Simon, I.; Dosztányi, Z. *Phys. Biol.* **2011**, *8*, 035003.
(32) Boehr, D. D.; Nussinov, R.; Wright, P. E. *Nat. Chem. Biol.* **2009**, *5*, 789−96.
(33) Wright, P.; Dyson, H. *J. Mol. Biol.* **1999**, *293*, 321−331.
(34) Campen, A.; Williams, R. M.; Brown, C. J.; Meng, J.; Uversky, V. N.; Dunker, A. K. *Protein Peptide Lett.* **2008**, *15*, 956−963.
(35) Lindorff-Larsen, K.; Trbovic, N.; Maragakis, P.; Piana, S.; Shaw, D. E. *J. Am. Chem. Soc.* **2012**, *134*, 3787−91.
(36) Ensign, D. L.; Kasson, P. M.; Pande, V. S. *J. Mol. Biol.* **2007**, *374*, 806−816.
(37) Noé, F.; Schütte, C.; Vanden-Eijnden, E.; Reich, L.; Weikl, T. R. *Proc. Natl. Acad. Sci. U. S. A.* **2009**, *106*, 19011−6.
(38) Bowman, G. R.; Voelz, V. A.; Pande, V. S. *Curr. Opin. Struct. Biol.* **2011**, *21*, 4−11.
(39) Sadiq, S.; Noé, F.; De Fabritiis, G. *Proc. Natl. Acad. Sci. U. S. A.* **2012**, *109*, 20449−20454.
(40) Buch, I.; Giorgino, T.; De Fabritiis, G. *Proc. Natl. Acad. Sci. U. S. A.* **2011**, *108*, 10184−9.
(41) Hilser, V. J. *Science* **2010**, *327*, 653−4.
(42) Tsai, C. J.; Ma, B.; Sham, Y. Y.; Kumar, S.; Nussinov, R. *Proteins* **2001**, *44*, 418−427.